Tumor Fusion Burden as a Hallmark of Immune Infiltration in Prostate Cancer

Marie-Claire Wagle[1], Joseph Castillo[1], Shrividhya Srinivasan[1], Thomas Holcomb[1], Kobe C. Yuen[1], Edward E. Kadel[1], Sanjeev Mariathasan[1], Daniel L. Halligan[2], Adrian R. Carr[2], Max Bylesjo[2], Paul R. McAdam[2], Sarah Lynagh[2], Koen M. Marien[3], Mark Kockx[3], Yannick Waumans[3], Shih-Min A. Huang[1], Mark R. Lackner[1], and Zineb Mounir[1]

ABSTRACT

Prostate cancer is the second leading cause of cancer-related death in men. Despite having a relatively lower tumor mutational burden than most tumor types, multiple gene fusions such as *TMPRSS2:ERG* have been characterized and linked to more aggressive disease. Individual tumor samples have been found to contain multiple fusions, and it remains unknown whether these fusions increase tumor immunogenicity. Here, we investigated the role of fusion burden on the prevalence and expression of key molecular and immune effectors in prostate cancer tissue specimens that represented the different stages of disease progression and androgen sensitivity, including hormone-sensitive and castration-resistant prostate cancer. We found that tumor fusion burden was inversely correlated with tumor mutational burden and not associated with disease stage. High fusion burden correlated with high immune infiltration, PD-L1 expression on immune cells, and immune signatures, representing activation of T cells and M1 macrophages. High fusion burden inversely correlated with immune-suppressive signatures. Our findings suggest that high tumor fusion burden may be a more appropriate biomarker than tumor mutational burden in prostate cancer, as it more closely associates with immunogenicity, and suggests that tumors with high fusion burden could be potential candidates for immunotherapeutic agents.

Introduction

Prostate cancer is the second leading cause of cancer-related death in men, with over 160,000 American men diagnosed each year (1). Following hormone therapy, castration-resistant prostate cancer (CRPC) may emerge, which represents the most aggressive form of the disease with the worst prognosis. CRPC can develop from non-metastatic or metastatic prostate cancer. Next-generation sequencing studies evaluating clinical CRPC samples have identified alterations in key regulatory pathways in prostate cancer including androgen signaling, PI3K signaling, and DNA repair pathways (2–4). However, the most common alterations in prostate cancer remain fusions of androgen-regulated promoters to members of the E26 transformation-specific (ETS) family of transcription factors such as *TMPRSS2:ERG*, found in 40%–50% of prostate cancer (5). These gene translocations are nonrandom events known to be driven and regulated by androgen receptor (AR; refs. 6, 7). In contrast, somatic point mutations are less frequent in prostate cancer compared with other solid tumors with a median tumor mutation burden (TMB) of 3.6 mutations/Mb and 7.7% of cases with more than 20 mutations/Mb placing prostate cancer on the lower TMB spectrum compared with other tumor types (8).

Studies in diverse cancers treated with various immunotherapies observed that higher TMB predicts favorable outcomes to PD-1/PD-L1 checkpoint blockade, although not universal in all tumor types (9), and is independently associated with better outcome (10). Unfortunately, apart from the approval of the vaccine sipuleucel-T in 2010 (11), immunotherapies including checkpoint blockade have been largely unsuccessful in prostate cancer due to the poor immunogenicity and low immune infiltrate in these tumors. This may change, however, as results from the phase 1b KEYNOTE-028 trial suggest that prostate cancer patients who are PD-L1 positive can derive durable responses with pembrolizumab (12). In addition, the phase II Checkmate 650 trial demonstrates increased response to nivolumab and ipilimumab in mCRPC with high TMB (13), further highlighting the need to improve our understanding of the immune landscape.

Our study aimed to assess the immune landscape in a prostate cancer tissue sample collection including both hormone-sensitive and CRPC cases, and to investigate the relationship between the immune microenvironment and the tumor genetic makeup. We observed that tumor fusion burden (TFB), a measure of the number of genetic fusions found in a tumor, inversely correlated with TMB in prostate cancer samples and that high TFB was linked to higher immune infiltration, higher PD-L1 expression on immune cells, and higher activation of T cells and M1 macrophages, whereas it inversely correlated with immune-suppressive signatures. Our findings suggested that TFB may be a more relevant biomarker than TMB in prostate cancer, where mutational load was generally very low and that high TFB may be more closely associated with higher immunogenicity, which may help identify patients with prostate cancer that respond to immunotherapeutic agents.

Materials and Methods

Diagnosis, disease stage, metastasis sites, and prior treatment of the tissue specimens can be found in Supplementary Table S1. Disease stage was determined using both TNM staging and Gleason score (14) according to the following criteria: early/intermediate

[1]Oncology Biomarker Development, Genentech, Inc., South San Francisco, California. [2]Fios Genomics, Nine Edinburgh Bioquarter, Edinburgh, United Kingdom. [3]HistoGeneX, Antwerp, Belgium.

Note: Supplementary data for this article are available at Cancer Immunology Research Online (http://cancerimmunolres.aacrjournals.org/).

Current address for M.-C. Wagle, M.R. Lackner, and Z. Mounir: IDEAYA Biosciences, South San Francisco, California; and current address for S.-M.A. Huang, Pharmacyclics, Sunnyvale, California.

Corresponding Authors: Zineb Mounir, IDEAYA Biosciences, 7000 Shoreline Court, Suite 350, South San Francisco, CA 94080. Phone: 617-645-8009; E-mail: zineb.mounir@mail.mcgill.ca; and Marie-Claire Wagle, mariewagle@gmail.com

Cancer Immunol Res 2020;8:844–50

doi: 10.1158/2326-6066.CIR-19-0568

(TNM: T1a–T2a/T2b–T2c; Gleason ≤6–7) and late (TNM: T3a–T4b; Gleason >7). An overview of the analyses performed along with information regarding which samples passed/failed each analysis are shown in Supplementary Table S2.

Derivation of TMB, TFB, and CRPC scores from RNA-sequencing data

Total RNA was isolated using miRNeasy Mini Kit with an on-column DNase digestion according to the manufacturer's protocol (Qiagen 217004). Library preparation and sequencing were performed at Q2 Solutions-EA genomics. To calculate TMB and TFB, paired-end RNA-sequencing (RNA-seq) data was aligned using STAR aligner (15) to the human genome (GRCh38) using the GENCODE v25 annotation. Opossum (16) was used to process the STAR aligner output prior to variant calling using Platypus (17). RNA-seq data can be found at the NCBI BioProject (accession no.: PRJNA624313) TMB was defined as the total number of variants identified after filtering to remove those in repetitive regions, low coverage regions, and those without an amino acid changing impact, relative to the average number of aligned bases. STARChip (18) was used to process the STAR aligner putative chimeric reads to identify the most likely fusion transcripts. "Fusion burden" was defined as the number of fusions identified per 10,000 genes profiled in a sample.

Because of the poor clinical annotation of the samples as either hormone-sensitive or castration-resistant, each sample was allocated a CRPC score using a published gene signature (19). Low scores reflect more hormone-sensitive specimens and high scores represent those that are castration resistant. The CRPC score was calculated using z-score–transformed expression of 150 core genes specifically regulated by AR only in CRPC tissues (19). CRPC scores were then derived from the first principal component to weight the score on the largest set of correlated genes. The distribution of TMB, TFB, and CRPC scores are shown in Supplementary Fig. S1A and the values for each sample are shown in Supplementary Table S3. Samples were categorized into quartiles for TMB, TFB, and CRPC scores with 25% samples placed in the lowest quartile, 25% in the highest quartile, and 50% in the intermediate quartile (Supplementary Fig. S1C). To assess the strongest associations between TFB and CRPC with molecular and immune signature scores, only samples in the lowest and highest quartile categories were included in the analyses.

Gene signature analyses

Gene signatures were identified from the literature and the genes contained in each signature are listed with relevant references in Supplementary Table S4 and scores for each sample are listed in Supplementary Table S3. For each signature, a single gene expression "score" was obtained for each sample using principal component analysis. Specifically, the z-scored first principal component of expression was calculated for the set of median centered gene expression levels for genes within each signature. Where required, the sign of the principal component was reversed to achieve a positive correlation with the mean z-scored expression levels to facilitate interpretation. This score is expected to capture the main trend of expression values within the gene list of interest.

IHC staining and image analysis

Antibodies used for IHC are shown in Supplementary Table S5 Stromal tumor-infiltrating lymphocytes (TIL) were assessed using an hematoxylin and eosin (H&E)–stained sample section. Stromal TILs were enumerated using methods and criteria established by Salgado and colleagues (20) and defined as the percent of desmoplastic stroma area [both intratumoral and contiguous peritumoral or intraepithelial (in BPH samples)] occupied by immune cells. Necrotic areas, which stained pink with the H&E stain and contained acellular material containing nonviable tumor cells, were excluded from the tumor area. Samples were categorized as having either low or high %TILs using a median cutoff of 3%. AR-positive cells were measured in PanCK-positive tumor parenchyma (or epithelial cells in the BPH samples) and PanCK-negative tumor stroma using VIS software (Visiopharm) from a whole-slide image of PanCK-AR–stained slides. PanCK, stained with Ventana DISCOVERY Purple kit (Roche; catalog no. 760-229) was used to classify the epithelial compartment. AR-positive cells were stained using the OptiView DAB IHC detection kit (Ventana; catalog no. 760-700). The PD-L1 (SP142) assay was purchased from Ventana. Slides were stained in a Clinical Laboratory Improvement Amendments–approved IHC laboratory at HistoGeneX with use of the FDA-approved SP142 assay and their respective protocols, which are detailed in the product inserts and autostainers (Ventana BenchMark Ultra, Roche; catalog no. N750-BMKU-FS 05342716001). The IC score is a relative area estimate, that is, the percentage of tumor area (or epithelial cells in the BPH samples) that is covered by PD-L1–positive ICs, which confers to the scoring approach described in the Ventana SP142 PD-L1 IHC assay brochure. PD-L1–stained TCs were scored in terms of the tumor proportion score (TPS), which represents the best estimated percentage (0%–100%) of TCs showing partial or complete membranous PD-L1 staining. TC and IC staining were binned into the following categories: IC0, 0–<1%; IC1, 1%–<5%; IC2, 5%–<10%; IC3, ≥10%; TC0, 0–<1%; TC1, 1%–<5%; TC2 5%–<50%; and IC3, ≥50%. All stained slides were scanned with the Panoramic SCAN 250 whole-slide scanner (3DHISTECH) under a 20× Plan Apo objective (0.80 numerical aperture) and a Hitachi (HV-F22CL) charge-coupled device progressive scan color camera with a resulting image resolution of 0.23 mm/pixel. Scans were analyzed using VIS software (version 6.6.1, Visiopharm).

IHC data

IHC values from stromal and tumor (epithelial) AR staining, PD-L1 staining on immune or tumor cells, and H&E staining for stromal TILs are shown in Supplementary Table S6.

Statistical analysis

Contrasts between categories including disease stages, CRPC scores, TFB scores, and CD8 low/high were assessed using parametric, two tailed, unpaired *t* tests with Welch correction (which does not assume equal sd) using GraphPad Prism (GraphPad Software Inc., version 8.2.1) unless otherwise noted. *P* values <0.05 were considered to be significant. Associations between continuous variables were assessed using Pearson correlation analysis. R^2 values of ≤−0.5 or ≥0.5 with associated *P* values ≤0.05 were considered to be significant.

Results

To evaluate the immune landscape in prostate cancer, we used a human tissue collection that comprises benign prostatic hyperplasia (BPH) tissues along with samples from early/intermediate (TNM: T1a–T2a and T2b–T2c; Gleason ≤6–7) and late (TNM: T3a–T4b; Gleason >7)–stage disease and metastatic tissue samples. Our RNA-seq analysis showed that TMB ranged from 0.01 to 1.2 mutations per Mb across all samples with a median of 0.5, lower than previously reported (6), whereas TFB ranged from 0 to 34 fusions/10,000 genes (up to 70 fusions per sample; Supplementary Fig. S1A). Fusions and mutations present in the samples are shown in Supplementary Tables

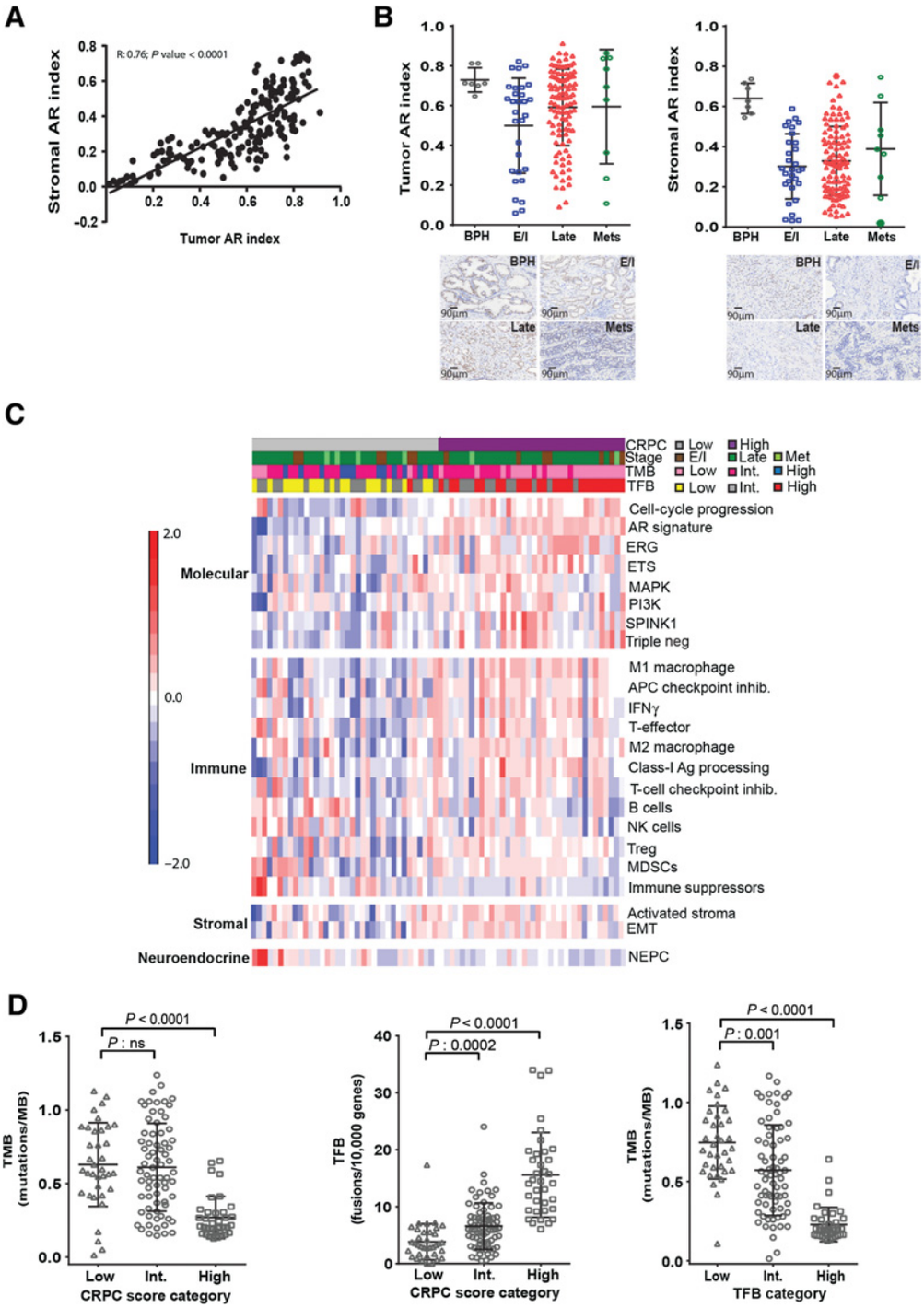

Figure 1.

Molecular profiling and characterization of the tumor mutation and fusion burden in prostate cancer tissue samples. **A,** Pearson correlation analysis of AR IHC staining in the tumor versus the stroma compartment. **B,** Quantification of tumor and stromal AR IHC staining across tumor stages, including benign prostatic hyperplasia (BPH; $n = 10$), early/intermediate (E/I; $n = 30$), and late-stage primary disease ($n = 123$) compared with metastatic samples (Mets; $n = 9$). Lines in scatter plots show the mean and standard deviation. Representative IHC images for AR (brown) for each disease stage as described above are shown; all samples were stained for AR. Scale bar for each image, 90 μm. **C,** RNA-seq analysis of all prostate cancer tissue samples ($n = 150$) and clustering based on CRPC scores (low vs. high; $n = 37$ samples per category) as specified in Materials and Methods. Disease stage, TMB, and TFB are also annotated across all samples. Gene signature analyses were performed as specified in Materials and Methods. Signature scores were correlated with CRPC scores from each patient using a Pearson correlation; **Table 1** shows correlation coefficients (R) and P values derived from this analysis. E/I, early/intermediate; EMT, epithelial-to-mesenchymal transition; inhib., inhibitor; Int., intermediate; MDSC, myeloid-derived suppressor cell; neg, negative; NK, natural killer; Treg, regulatory T cell. **D,** Analysis of TMB (mutations per MB) and TFB (fusions per 10,000 genes) in relation to CRPC score categories [low ($n = 37$), intermediate ($n = 76$), and high ($n = 37$)] as defined in the Materials and Methods. Lines in scatter plots show the mean and SD. P values were calculated using a two-tailed, unpaired t test with Welch correction. Int., intermediate; ns, not significant.

Table 1. Correlation of signature scores to CRPC scores.

Signature	*R* coefficient	*P*
AR	0.829	2.3E-19
PI3K	0.522	2.6E-06
ERG	0.441	1.0E-04
ETS	0.422	2.2E-04
Triple negative (ERG-ETS-SPINK1)	0.421	2.3E-04
Class-I antigen processing	0.585	6.8E-08
Activated stroma	0.481	1.9E-05
Natural killer cells	−0.314	7.3E-03
Immune suppressors	−0.634	2.2E-09
NEPC gene classifier	−0.729	2.0E-13

S7 and S8, respectively. As expected, TMB, TFB, and CRPC scores were lower in BPH samples compared with the prostate cancer samples and there were no significant differences in these values between disease stages (Supplementary Fig. S1B). IHC assessment of androgen receptor (AR) expression showed that tumor and stromal AR expression were strongly correlated ($R = 0.76$; $P < 0.0001$; **Fig. 1A**). Reduction of AR expression seemed to occur between BPH and prostate cancer disease progression as described previously (ref. 21; **Fig. 1B**). To assess changes in molecular and immune expression signatures with tumor hormone sensitivity and castration-resistant samples were allocated a CRPC score and categorized into quartiles (see Materials and Methods, Supplementary Fig. S1A and S1C). Gene expression signature data from the lowest and highest CRPC quartiles, representing the most hormone-sensitive versus the most castration-resistant samples, respectively, were clustered separately (**Fig. 1C**). High CRPC scores correlated with AR signaling although there were small differences in stromal and tumor AR expression between the high and low quartiles (**Fig. 1C**; **Table 1**; Supplementary Fig. S1D). High CRPC scores also correlated with high PI3K signaling, class 1A antigen processing and activated stromal signature scores, and inversely correlated with signatures representing neuroendocrine biology and immune suppressors suggesting potentially enhanced immunogenicity (**Fig. 1C**; **Table 1**). Interestingly, samples with high CRPC scores had low TMB, whereas samples with low CRPC scores had higher and more variable TMB with a wider range (TMB in CRPC low vs. high: $P < 0.0001$). CRPC scores correlated strongly with TFB ($P < 0.0001$) and ERG/ETS transcriptional signatures (**Fig. 1C** and **D**). TMB was also inversely correlated with TFB ($P < 0.0001$) across all samples (**Fig. 1D**).

To investigate whether TFB rather than TMB was associated with enhanced immunogenicity, signature data from low and high TFB quartiles were clustered separately (**Fig. 2A**). Samples with high TFB showed enhanced expression of immune signatures representing activation of M1 macrophages, checkpoint inhibitors, IFNγ-induced T-cell activity, T-effector activation, and class I antigen processing, whereas inversely correlating with immune suppressor signatures (**Fig. 2A**; **Table 2**). High TFB also correlated with cell-cycle progression and AR signaling, as well as ERG and ETS transcriptional activity (**Fig. 2A**; **Table 2**). About 40% of the tissue collection samples harbored ERG fusions (Supplementary Table S7) allowing the categorization of all samples as either ERG fusion positive or ERG fusion negative. ERG fusion–positive samples were found to have a significantly higher overall fusion burden ($P < 0.0002$) with correspondingly higher ERG transcriptional activity compared with ERG fusion–negative samples ($P < 0.0001$; Supplementary Fig. S1E).

Assessment of TILs in the stroma of the invasive margin and central tumor area combined showed that approximately half of the samples (17/36; 47%) with low TFB had <3% TILs, whereas most samples (25/36; 69%) with high TFB had ≥3% TILs (**Fig. 2B**; $P = 0.0006$; images in **Fig. 2C**). T-cell activation was similar in all the samples with low TFB regardless of %TILs compared with the samples with high TFB (**Fig. 2D**). Samples with high TFB and ≥3% TILs had significantly higher T-cell activation scores than those with low or high TFB and <3% TILs ($P = 0.0003$ and $P = 0.04$, respectively). These data suggest that the few TILs present in the low TFB samples seem less active than those found in high TFB samples.

Samples with high TFB also showed higher PD-L1 expression on the immune ICs (**Fig. 2E** and **F**; $P = 0.02$ for ≥IC1 between low and high TFB), whereas PD-L1 expression on tumor cells was negative (Supplementary Table S6). Percent TILs did not significantly change across disease stage; however, PD-L1 expression significantly increased between BPH and all the prostate cancer disease stages (≥IC1: $P < 0.0001$), although there were no significant differences between the disease stages (Supplementary Fig. S1F and S1G). IC3-positive PD-L1 samples were only in the late and metastatic samples; however, this represented only three samples in the whole collection (Supplementary Fig. S1G). Our findings showed that prostate cancer samples with high TFB also have high CRPC scores. In addition, our results demonstrated that prostate cancer samples with high TFB also have elevated immune infiltration and enhanced immunogenicity pointing to TFB as a relevant biomarker that may help identify patients with prostate cancer more likely to respond to immunotherapy agents.

Discussion

In our quest to assess the immune landscape in prostate cancer and investigate the relationship between the immune microenvironment and tumor molecular makeup, we found that TFB inversely correlated with TMB and that high TFB correlated with a high % of activated TILs, high PD-L1 expression, high T-cell and M1 macrophage activation; however, TFB inversely correlated with immune suppressive signatures. Pan-tumor type immune studies have linked TMB to checkpoint inhibitor response and disease outcome (10). However, compared with other tumor types, prostate cancer remains a low TMB disease with minimal success of immunotherapeutic agents apart from cancer vaccines that function by promoting immune infiltration and activation within the prostate cancer tumors (8). Despite prostate cancer having a relatively low TMB, a pembrolizumab phase Ib trial shows that PD-L1–positive patients with prostate cancer derive benefit with durable responses (12). In this and similar trials, it would be highly valuable to assess TFB in these patients in correlation with response.

Upon resistance to hormone therapy, prostate cancer evolves into CRPC, a very aggressive disease characterized by low TMB with alterations in key regulatory pathways including PI3K and androgen pathways (3). Whereas remaining low in TMB, about 50% of these tumors carry gene fusions whose presence seems to correlate with poor prognosis (22). Gene mutations and fusions are regulated through very different DNA repair pathways with nonhomologous end joining (NHEJ), an error-prone mechanism of DNA double strand breaks (DSB) repair, being a major DNA repair pathway producing gene fusions. The presence of genomic aberrations that interfere with DNA repair in castration-resistant prostate cancer show clinical responses to PARP inhibitors (23, 24). In agreement with our data, tumors harboring a high number of fusion events tend to have lower mutational

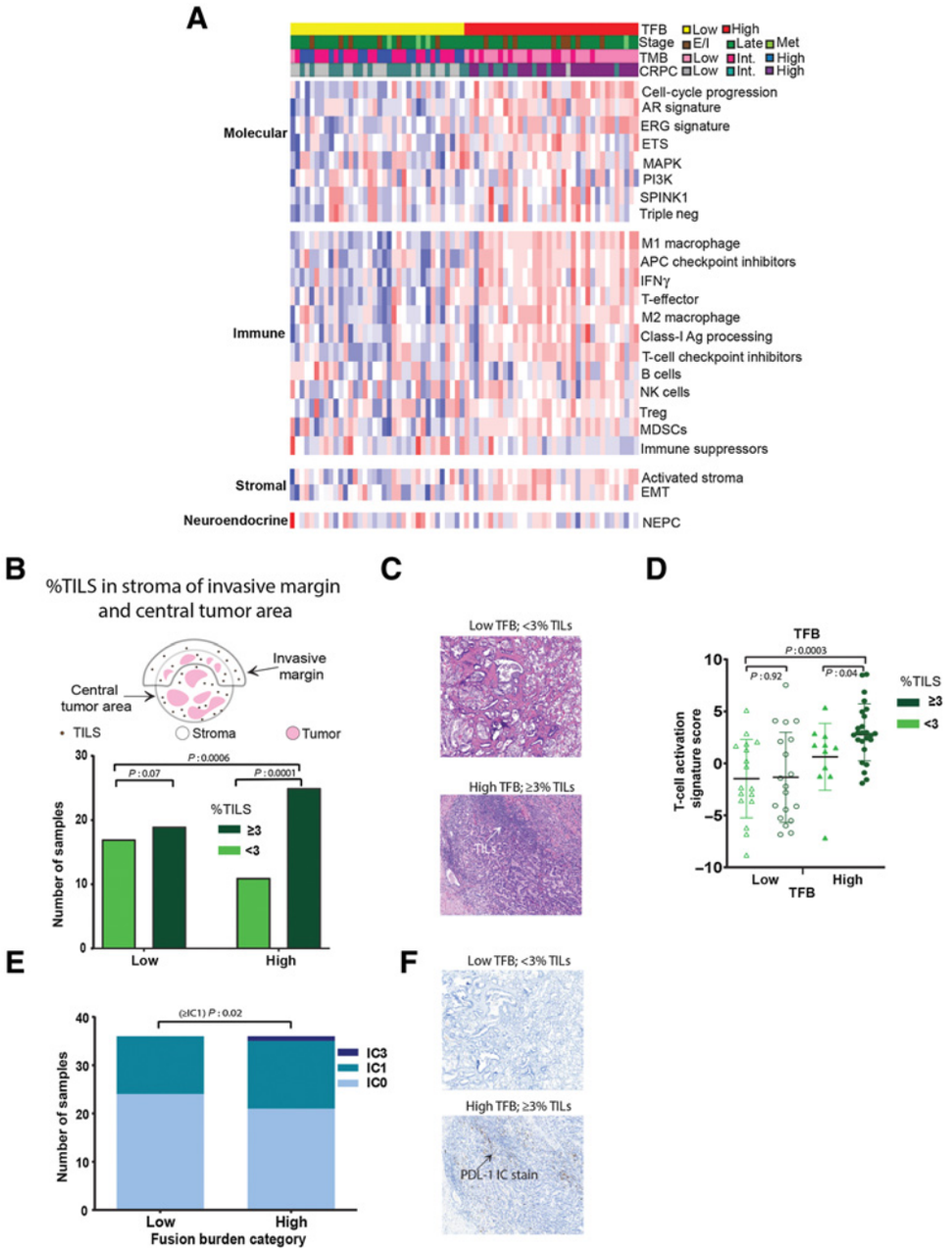

Figure 2.

Immune profiling of prostate cancer tissues and relationship between immune infiltration and tumor fusion burden. **A,** RNA-seq analysis of all prostate cancer tissue samples and clustering based on fusion burden (low vs. high, $n = 37$ for each category). Disease stage, TMB, and CRPC scores are also annotated across all samples. Gene signature analyses were performed as specified in Materials and Methods. Signature scores were correlated with TFB values across all patients using a Pearson correlation; **Table 2** shows correlation coefficients (R) and P values derived from this analysis. E/I, early/intermediate; EMT, epithelial-to-mesenchymal transition; inhib., inhibitor; Int., intermediate; MDSC, myeloid-derived suppressor cell; neg, negative; NK, natural killer; Treg, regulatory T cell. **B,** Stromal TILs were assessed using H&E-stained sample sections as specified in Materials and Methods. TILs were calculated as a percentage and defined into two categories (<3% TILs or ≥3% TILs according to median cutoff; 37 samples in each category). Histograms show the number of samples in either the <3% TILS or ≥3% TILS categories for samples with either high or low TFB; the P values of %TILs in the low versus high TFB category were calculated using a two-tailed, unpaired t test with Welch correction. **C,** Representative images of H&E staining showing high %TILs in a sample with high TFB ($n = 25$) compared with low %TILS in a sample with low TFB ($n = 17$). **D,** T-cell activation scores in samples with low or high TFB with either <3 or ≥3% TILs. P values were calculated using a two-tailed, unpaired t test with Welch correction **E,** PD-L1 IHC staining using antibody SP142, which only recognizes immune cells positive for PD-L1, was quantified and categorized as specified into IC0, IC1, IC2, and IC3 categories ($n = 180$). Histogram shows the number of samples in each PD-L1 staining category, IC0, IC1, or IC3, in either the fusion burden low or high groups. P value from comparison of number of samples with ≥IC1 staining between low and high TFB and calculated using a two-tailed, unpaired t test with Welch correction. There were no samples in the IC2 category. **F,** Representative images showing PD-L1 (≥IC1) staining in samples with high TFB ($n = 15$) compared with high PDL-1 (≥IC1) in samples with low TFB ($n = 12$).

Table 2. Correlation of signature scores to TFB.

Signature	*R* coefficient	*P*
M1 macrophage	0.594	3.7E-08
Cell-cycle progression	0.567	2.1E-07
APC checkpoint inhibitors	0.498	8.4E-06
AR	0.485	1.5E-05
IFNγ induced	0.464	4.0E-05
ERG	0.432	1.5E-04
T-cell checkpoint inhibitors	0.425	2.0E-04
T-effector	0.417	2.7E-04
M2 macrophage	0.401	4.8E-04
Class-I antigen processing	0.397	5.6E-04
Activated stroma	0.356	2.1E-03
ETS	0.329	4.7E-03
Immune suppressors	−0.317	6.7E-03

burden (25), and prostate cancer tumors with *CDK12* loss leads to increased gene fusions, neoantigen burden, and T-cell infiltration (26). While much progress has been made to identify point mutations and deletions that can generate novel epitopes or neoantigens that can form MHC-I epitopes, there are other potential tumor neoantigens to be identified, including those emerging from tumor gene fusions. A novel automated gene fusion neoantigen discovery pipeline, INTEGRATE-Neo, complements the existing knowledge in mutation-driven neoantigen production and prediction (27). Our findings suggest that fusion-positive prostate cancer, although considered a cancer with a low TMB, may still harbor many neoantigens potentially from gene fusions, which may serve as targets for immunotherapy as has been shown in soft-tissue malignancies (28). Our findings suggested that TFB may be a more relevant biomarker than TMB in prostate cancer and that through its association with high immune infiltration and activation within the tumor, TFB may help identify patients with prostate cancer more likely to respond to immunotherapeutic agents. Large-scale studies in prostate cancer and CRPC patient tissue samples assessing the prevalence and role of gene fusions in the context of the existing clinical immunotherapy studies would be needed to fully validate the use of TFB as a predictive biomarker in prostate cancer. A limitation of our study is the lack of clinical annotation of the samples characterized for TFB and other molecular markers including treatment history and clinical response, which are not routinely collected by tissue procurement banks. As such, further validation of this study could include a larger scale prevalence assessment in clinically annotated prostate cancer and CRPC patient samples to enable the correlation of TFB with treatment response and relapse following castration therapy. Our study identified high TFB as a novel biomarker in prostate cancer as it more closely associated with immunogenicity and may be predictive of clinical response to immunotherapeutic agents.

Disclosure of Potential Conflicts of Interest

J. Castillo is Senior Scientific Researcher at Genentech, Inc. S. Srinivasan is Clinical Biomarker Operations Leader at Genentech, Inc. K.C. Yuen is Associate Scientist at Genentech, Inc. E.E. Kadel is Principal Scientific Researcher at Genentech, Inc. S. Mariathasan is Principal Scientist at Genentech, Inc. D.L. Halligan, A.R. Carr, M. Bylesjo, and P.R. McAdam are employees of Fios Genomics, a contract research organization contracted to provide bioinformatics services to Genentech, Inc. K.M. Marien is a histoscientist at HistoGeneX. Y. Waumans is Section Head, Pathology, Imaging and Quantification at HistoGeneX. S.-M.A. Huang is an associate director at Genentech/Roche. M.R. Lackner is a director at Roche. Z. Mounir is an associate director at IDEAYA Biosciences. No potential conflicts of interest were disclosed by the other authors.

Authors' Contributions

Conception and design: M.-C. Wagle, S.-M.A. Huang, Z. Mounir
Development of methodology: M.-C. Wagle, K.C. Yuen, P.R. McAdam, K.M. Marien, M. Kockx, Y. Waumans, Z. Mounir
Acquisition of data (provided animals, acquired and managed patients, provided facilities, etc.): J. Castillo, S. Srinivasan, T. Holcomb, Y. Waumans
Analysis and interpretation of data (e.g., statistical analysis, biostatistics, computational analysis): M.-C. Wagle, K.C. Yuen, E.E. Kadel, S. Mariathasan, D.L. Halligan, A.R. Carr, M. Bylesjo, P.R. McAdam, S. Lynagh, K.M. Marien, Y. Waumans, M.R. Lackner, Z. Mounir
Writing, review, and/or revision of the manuscript: M.-C. Wagle, J. Castillo, S. Srinivasan, T. Holcomb, E.E. Kadel, S. Mariathasan, S.-M.A. Huang, M.R. Lackner, Z. Mounir
Administrative, technical, or material support (i.e., reporting or organizing data, constructing databases): S. Srinivasan, E.E. Kadel, Z. Mounir
Study supervision: Z. Mounir

Acknowledgments

The authors thank Steve Gendreau, Rich Price, and Jennifer Giltnane for helpful discussions. The authors also acknowledge Jeffrey Eastham-Anderson for his help with the IHC images.

Received July 24, 2019; revised November 1, 2019; accepted April 17, 2020; published first April 22, 2020.

References

1. Siegel RL, Miller KD, Jemal A. Cancer statistics, 2018. CA Cancer J Clin 2018;68:7–30.
2. Armenia J, Wankowicz SAM, Liu D, Gao J, Kundra R, Reznik E, et al. The long tail of oncogenic drivers in prostate cancer. Nat Genet 2018;50:645–51.
3. Robinson D, Van Allen EM, Wu Y-M, Schultz N, Lonigro RJ, Mosquera J-M, et al. Integrative clinical genomics of advanced prostate cancer. Cell 2015;162:454.
4. Zehir A, Benayed R, Shah RH, Syed A, Middha S, Kim HR, et al. Mutational landscape of metastatic cancer revealed from prospective clinical sequencing of 10,000 patients. Nat Med 2017;23:703–13.
5. Tomlins SA, Rhodes DR, Perner S, Dhanasekaran SM, Mehra R, Sun XW, et al. Recurrent fusion of TMPRSS2 and ETS transcription factor genes in prostate cancer. Science 2005;310:644–8.
6. Lin C, Yang L, Tanasa B, Hutt K, Ju B, Ohgi K, et al. Nuclear receptor-induced chromosomal proximity and DNA breaks underlie specific translocations in cancer. Cell 2009;139:1069–83.
7. Mani R-S, Tomlins SA, Callahan K, Ghosh A, Nyati MK, Varambally S, et al. Induced chromosomal proximity and gene fusions in prostate cancer. Science 2009;326:1230.
8. Chalmers ZR, Connelly CF, Fabrizio D, Gay L, Ali SM, Ennis R, et al. Analysis of 100,000 human cancer genomes reveals the landscape of tumor mutational burden. Genome Med 2017;9:34.
9. Maia MC, Almeida L, Bergerot PG, Dizman N, Pal SK. Relationship of tumor mutational burden (TMB) to immunotherapy response in metastatic renal cell carcinoma (mRCC). J Clin Oncol 36, 2018 (suppl 6S; abstr 662).
10. Goodman AM, Kato S, Bazhenova L, Patel SP, Frampton GM, Miller V, et al. Tumor mutational burden as an independent predictor of response to immunotherapy in diverse cancers. Mol Cancer Ther 2017;16:2598–608.
11. Kantoff PW, Higano CS, Shore ND, Berger ER, Small EJ, Penson DF, et al. Sipuleucel-T immunotherapy for castration-resistant prostate cancer. N Engl J Med 2010;363:411–22.
12. Hansen AR, Massard C, Ott PA, Haas NB, Lopez JS, Ejadi S, et al. Pembrolizumab for advanced prostate adenocarcinoma: findings of the KEYNOTE-028 study. Ann Oncol 2018;29:1807–13.
13. Sharma P, Pachynski RK, Narayan V, Flechon A, Gravis G, Galsky MD, et al. Initial results from a phase II study of nivolumab (NIVO) plus ipilimumab (IPI)

for the treatment of metastatic castration-resistant prostate cancer (mCRPC; CheckMate 650). J Clin Oncol 37, 2019 (suppl 7S; abstr 142).
14. Herden J, Heidenreich A, Wittekind C, Weissbach L. Predictive value of the UICC and AJCC 8th edition tumor-nodes-metastasis (TNM) classification for patients treated with radical prostatectomy. Cancer Epidemiol 2018;56: 126–32.
15. Dobin A, Davis CA, Schlesinger F, Drenkow J, Zaleski C, Jha S, et al. STAR: ultrafast universal RNA-seq aligner. Bioinformatics 2013;29:15–21.
16. Oikkonen L, Lise S. Making the most of RNA-seq: pre-processing sequencing data with Opossum for reliable SNP variant detection. Wellcome Open Res 2017;2:6.
17. Rimmer A, Phan H, Mathieson I, Iqbal Z, Twigg SRF, WGS500 Consortium, et al. Integrating mapping-, assembly- and haplotype-based approaches for calling variants in clinical sequencing applications. Nat Genet 2014;46: 912–8.
18. Akers NK, Schadt EE, Losic B. STAR Chimeric Post for rapid detection of circular RNA and fusion transcripts. Bioinformatics 2018;34:2364–70.
19. Sharma NL, Massie CE, Ramos-Montoya A, Zecchini V, Scott HE, Lamb AD, et al. The androgen receptor induces a distinct transcriptional program in castration-resistant prostate cancer in man. Cancer Cell 2013;23:35–47.
20. Salgado R, Denkert C, Demaria S, Sirtaine N, Klauschen F, Pruneri G, et al. The evaluation of tumor-infiltrating lymphocytes (TILs) in breast cancer: recommendations by an International TILs Working Group 2014. Ann Oncol 2015;26: 259–71.
21. Filipovski V, Kubelka-Sabit K, Jasar D, Janevska V. Androgen receptor expression in epithelial and stromal cells of prostatic carcinoma and benign prostatic hyperplasia. Open Access Maced J Med Sci 2017;5:608–12.
22. Kumar-Sinha C, Tomlins SA, Chinnaiyan AM. Recurrent gene fusions in prostate cancer. Nat Rev Cancer 2008;8:497–511.
23. Grasso CS, Wu Y-M, Robinson DR, Cao X, Dhanasekaran SM, Khan AP, et al. The mutational landscape of lethal castration-resistant prostate cancer. Nature 2012;487:239–43.
24. Mateo J, Carreira S, Sandhu S, Miranda S, Mossop H, Perez-Lopez R, et al. DNA-repair defects and olaparib in metastatic prostate cancer. N Engl J Med 2015;373: 1697–708.
25. Gao Q, Liang W-W, Foltz SM, Mutharasu G, Jayasinghe RG, Cao S, et al. Driver fusions and their implications in the development and treatment of human cancers. Cell Rep 2018;23:227–38.
26. Wu Y-M, Cieślik M, Lonigro RJ, Vats P, Reimers MA, Cao X, et al. Inactivation of CDK12 delineates a distinct immunogenic class of advanced prostate cancer. Cell 2018;173:1770–82.
27. Zhang J, Mardis ER, Maher CA. INTEGRATE-neo: a pipeline for personalized gene fusion neoantigen discovery. Bioinformatics 2017;33:555–7.
28. Worley BS, van den Broeke LT, Goletz TJ, Pendleton CD, Daschbach EM, Thomas EK, et al. Antigenicity of fusion proteins from sarcoma-associated chromosomal translocations. Cancer Res 2001;61:6868–75.
29. Mariathasan S, Turley SJ, Nickles D, Castiglioni A, Yuen K, Wang Y, et al. TGFβ attenuates tumour response to PD-L1 blockade by contributing to exclusion of T cells. Nature 2018;554:544–8.